UDC 550.340

Andriy GNYP, Dmytro MALYTSKYY

Carpathian Branch of Subbotin Institute of Geophysics, National Academy Sciences of Ukraine, 3B, Naukova str., Lviv, 79060, Ukraine, e-mail: agnyp.gm@gmail.com, https://orcid.org/0000-0002-2612-4234

https://doi.org/10.23939/jgd2023.02.019

RELOCATING EARTHQUAKES IN CLUSTERS BASED ON VARIATIONS IN THE INTERVALS BETWEEN THEIR FIRST *P*- AND *S*-WAVES

The length of the interval between the first *P*- and *S*-waves is routinely used as a rough estimator of epicentral distance. We propose an algorithm for the relocation of earthquakes occurring in clusters, based on the simultaneous comparison of a large number of intervals. Variations in the intervals at each station are measured by cross-correlation between the respective portions of records directly and without a reference to any absolute times. In the current version of the algorithm, it is assumed that the size of the cluster is much smaller than the distance to the stations; the azimuths of the stations, as well as the angles of the emergence of the first *P*- and *S*-waves, are more or less accurately known for at least one (reference) earthquake; and the rays of the first waves lie in the vertical plane that contains the earthquake and the station. Under these assumptions, the relationship between the locations and the variations in the intervals becomes purely geometrical and linear, and the corresponding system can easily be solved. A series of synthetic experiments with different numbers and configurations of stations, levels of noise in the observed data, sparse data, and inaccuracies in azimuths and angles of emergence have demonstrated the stable and reliable performance of the algorithm and its potential applicability to real data. Due to the large number of constraints on each location, the algorithm can be used primarily in the case of small earthquakes or sparse networks when a large portion of data is missing. It can be used independently, to validate the locations determined by other methods, or be integrated into them, thereby improving their reliability by providing a large number of additional constraints.

Key words: earthquake locations; relocation; cluster earthquakes; interval between first *P*- and *S*-waves; cross-correlation.

Introduction

Small earthquakes, much more frequent than large ones, provide a wealth of invaluable information for many applications of seismological research. Recent staggering advances in real-time access to an ever-increasing volume of seismological data make their use even more feasible. The problem of improving the location accuracy of small earthquakes has remained the focus of seismological research for many decades. Although a wide variety of approaches have been proposed, most of them are based on exploiting the similarity of the waveforms of small earthquakes occurring in clusters. In earlier works, the differential arrivals of *P*- and/or *S*-waves corresponding to the cross-correlation maxima with the so-called *master* event were most often estimated [Shearer, 1997; Shearer et al., 2005]. Double differences between travel times for pairs of events were then introduced, minimizing the problem of spurious absolute arrivals, especially of *S*-waves, as well as the problem of a poorly known velocity structure [Waldhauser et al., 2000]. On the other hand, the absolute values of the cross-correlation between body waves [Menke, 1999] and coda waves [Sneider & Vrijlandt, 2005] were implemented in estimators of source separation between two earthquakes that can be used to locate earthquakes with a single station [Robinson, et al., 2007, 2013; Gnyp, 2013, 2014]. Often, the performance of the approaches can be further improved by combining them with each other as well as with more traditional location algorithms [Harris & Douglas, 2021].

When relocating earthquake clusters in the Carpathian region of Ukraine [Gnyp, 2010, 2022; Gnyp & Malytskyy, 2021], we also analyzed the variations in the differential intervals between the first *P*- and *S*-waves at each station and found that they correlated well with the changes in location obtained by using the differential arrival times of only *P*-waves. Although the analysis was then considered only auxiliary, the idea arose that the variations in *S*-to-*P* intervals themselves could be used to locate earthquakes. The advantage of variations seemed to be that they were not only independent of the source times but even of the absolute values of the intervals themselves and could easily be measured by the cross-correlation between the corresponding waveforms.

Algorithm

By comparing the intervals between the first *P*- and *S*-waves, one can judge which of the earthquakes is closer to the station; by comparing them at different

stations, roughly estimate the location of the earthquake. Our algorithm is based on the simultaneous comparison of the intervals for a large number of earthquakes. The difference $DDSP_{ij}^{(k)}$ between the intervals for a pair of earthquakes i and j at station k is defined as

$$\begin{aligned} DDSP_{ij}^{(k)} &= t_i^{(k)} + S_i^{(k)} - (t_i^{(k)} + P_i^{(k)}) - (t_j^{(k)} + S_j^{(k)}) + t_j^{(k)} + P_j^{(k)}, \\ &= S_i^{(k)} - S_j^{(k)} - (P_i^{(k)} - P_j^{(k)}), \\ &= DS_{ij}^{(k)} - DP_{ij}^{(k)}, \end{aligned}$$

in which t_i and t_j are the source times, $S_i^{(k)}$, $S_j^{(k)}$, $P_i^{(k)}$, and $P_j^{(k)}$ are the travel times of first P- and S-waves, $DP_{ij}^{(k)}$ and $DS_{ij}^{(k)}$ are the travel time differences between earthquakes i and j measured by the cross-correlation between the corresponding waveforms at station k, i, j = 1,…, N, and k = 1,….K. For N earthquakes, there will be $N(N\text{-}1)$ pairs and the same number (or sometimes lesser) of differences (observations) at each station.

Before establishing the dependence of the difference between the P- and S-wave intervals for a pair of earthquakes on their coordinates in the local Cartesian system (Northing, Easting, Z), we assume that since the cluster size is much smaller than the distance to the station, (i) the ray paths are almost identical outside the cluster, and the travel time differences arise inside the cluster and are the same as at the station; (ii) the changes in the station azimuth and angles of the emergence of P- or S-waves due to changes in the location are very small and can be neglected. It is also assumed that the rays lie in a vertical plane containing the earthquake and the station, and P- and S-wave velocities (v_P and v_S) are known and uniform within the cluster.

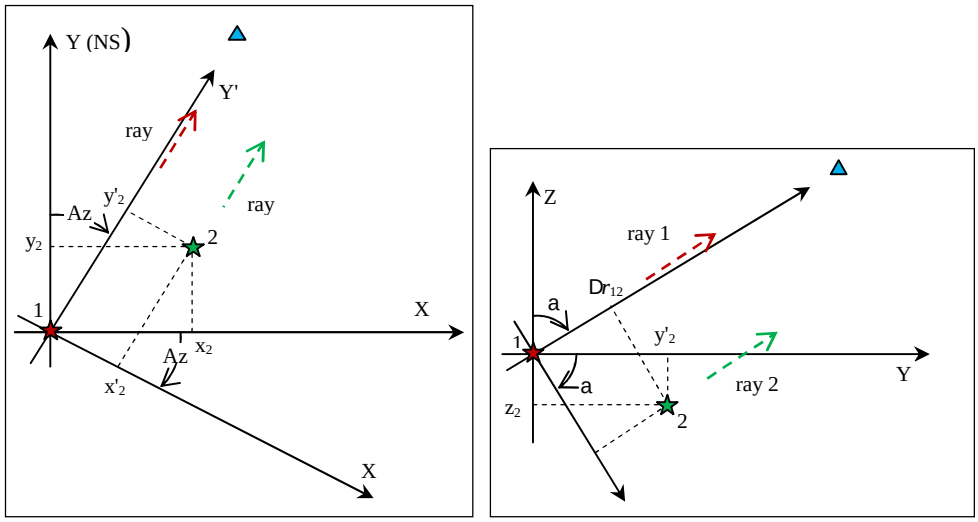

a b

Fig. 1. A scheme for the calculation of difference between the ray paths from earthquakes 1 and 2 with coordinates x_1, y_1, z_1, and x_2, y_2, z_2 in the local Cartesian system. A horizontal projection is on the (a), and a vertical one is on the (b). Earthquakes are indicated by red and green stars, and the station that is actually much further away is indicated by a blue triangle. a is the angle of emergence.

Then, at station k, the differences $D_a r_{12}^{(k)}$ and $D_b r_{12}^{(k)}$ between the ray paths of the first P- and S-waves with angles of emergence $\alpha^{(k)}$ and $\beta^{(k)}$ can be calculated for earthquakes 1 and 2 from their coordinates x_1, y_1, z_1, and x_2, y_2, z_2 in the local Cartesian system, as shown in Fig. 1. Since earthquake 1 is placed at the zero coordinates (x_1, y_1, z_1 ° 0), the horizontal projection of $D_a r_{12}^{(k)}$ can be obtained as a radial coordinate in the system rotated by the station's azimuth $Az^{(k)}$ (Fig. 1, *a*):

$$y_2^{'} = -x_2 \sin(-Az^{(k)}) + y_2 \cos(-Az^{(k)}),$$

in which $y_2^{'}$ is the horizontal projection of $D_a r_{12}^{(k)}$. Similarly (Fig. 1, *b*), $D_a r_{12}^{(k)}$ itself is calculated by rotating the system in the vertical plane by the angle of emergence ($\alpha^{(k)}$ or $\beta^{(k)}$):

$$D_a r_{12}^{(k)} = -y_2^{'} \sin(-\alpha^{(k)}) + z_2 \cos(-\alpha^{(k)}),$$

and

$$D_a r_{12}^{(k)} = -(-x_2 \sin(-Az^{(k)}) + y_2 \cos(-Az^{(k)})) \sin(-\alpha^{(k)}) + z_2 \cos(-\alpha^{(k)}), \quad (1)$$

with the axis Z directed upwards.

For a pair i and j, $D_a r_{ij}^{(k)}$ can be obtained in a system with zero coordinates translated to x_i, y_i, z_i:

$$D_a r_{ij}^{(k)} = -(-(x_j - x_i)\sin(-Az^{(k)}) + (y_j - y_i)\cos(-Az^{(k)}))\sin(-\alpha^{(k)}) + (z_j - z_i)\cos(-\alpha^{(k)}).$$

Then, since

$$DS_{ij}^{(k)} - DP_{ij}^{(k)} = D_b r_{ij}^{(k)} / v_S - D_a r_{ij}^{(k)} / v_P,$$

$$DDSP_{ij}^{(k)} = (((x_j - x_i)\sin(-Az^{(k)}) - (y_j - y_i)\cos(-Az^{(k)}))\sin(-\beta^{(k)}) + (z_j - z_i)\cos(-\beta^{(k)}))/v_S - (((x_j - x_i)\sin(-Az^{(k)}) - (y_j - y_i)\cos(-Az^{(k)}))\sin(-\alpha^{(k)}) + (z_j - z_i)\cos(-\alpha^{(k)}))/v_P. \quad (2)$$

After introducing the expressions

$$da^{(k)} = \sin(-Az^{(k)})\sin(-\beta^{(k)})/v_S - \sin(-Az^{(k)})\sin(-\alpha^{(k)})/v_P,$$
$$db^{(k)} = -\cos(-Az^{(k)})\sin(-\beta^{(k)})/v_S + \cos(-Az^{(k)})\sin(-\alpha^{(k)})/v_P, \quad (3)$$
$$dc^{(k)} = \cos(-\beta^{(k)})/v_S - \cos(\alpha^{(k)})/v_P,$$

we obtain the more compact expressions for the differences (2):

$$DDSP_{ij}^{(k)} = da^{(k)}(x_j - x_i) + db^{(k)}(y_j - y_i) + dc^{(k)}(z_j - z_i). \quad (4)$$

The equations (4) are linear with respect to the coordinates, and can be easily solved if angles $\alpha^{(k)}$ and $\beta^{(k)}$, and $Az^{(k)}$ are known.

After introducing vectors

$$\mathbf{X} = (x_2, y_2, z_2, x_3, y_3, z_3, \ldots, x_N, y_N, z_N)^T, \quad (5)$$

and $\mathbf{DDSP}^{(k)} = (DDSP_{12}^{(k)}, DDSP_{13}^{(k)}, \ldots, DDSP_{1N}^{(k)}, DDSP_{23}^{(k)}, DDSP_{24}^{(k)}, \ldots, DDSP_{2N}^{(k)}, \ldots, DDSP_{N-2N-1}^{(k)}, DDSP_{N-2N}^{(k)}, DDSP_{N-1N}^{(k)})^T$, (6)

equations (4) can be presented in matrix form:

$$\mathbf{D}^{(k)}\mathbf{X} = \mathbf{\Delta\Delta SP}^{(k)}, \quad (7)$$

in which the matrix $\mathbf{D}^{(k)}$ consists of the expressions (3) for $a^{(k)}$, $b^{(k)}$ and $c^{(k)}$, and its dimensions are $(N-1)\cdot N/2 \times 3\cdot(N-1)$. The structure of the system is transcribed in Appendix 1.

After introducing matrix **D** and vector **DDSP**

$$\mathbf{D} = \begin{bmatrix} \mathbf{D}^{(1)} \\ \mathbf{D}^{(2)} \\ \vdots \\ \mathbf{D}^{(K)} \end{bmatrix} \quad \mathbf{\Delta\Delta SP} = \begin{bmatrix} \mathbf{\Delta\Delta SP}^{(1)} \\ \mathbf{\Delta\Delta SP}^{(2)} \\ \vdots \\ \mathbf{\Delta\Delta SP}^{(K)} \end{bmatrix}$$

the system of equations for *K* stations is obtained:

$$\mathbf{DX} = \mathbf{\Delta\Delta SP}, \quad (8)$$

in which the dimensions of matrix **D** are $K\cdot(N-1)\cdot N/2 \times 3\cdot(N-1)$.

Locations **X** of the earthquakes relative to earthquake 1 can be obtained by solving the linear system (8):

$$\mathbf{X} = \mathbf{D}^{-1}\mathbf{\Delta\Delta SP}. \quad (9)$$

Synthetic experiments

Next, we conducted a series of synthetic experiments to test the performance of the algorithm depending on the number and configuration of stations, level of noise in the observed data, data sparsity, and inaccuracy of azimuths and angles of emergence. In these experiments, the synthetic earthquakes were located randomly along the two 3D lines intersecting at zero coordinates, thus defining an imaginary rupture plane (Table 1, Fig. 2). Variations in the intervals between *S*- and *P*-waves were generated for the original locations and used subsequently to recover the locations by solving the corresponding linear system.

Table 1

Coordinates of synthetic earthquakes in the local Cartesian system

	EW, km	NS, km	Z, km
1	0.00	0.00	0.00
2	9.00	9.00	9.00
3	–1.00	–1.00	–1.00
4	–2.00	–2.00	–2.00
5	8.00	8.00	8.00
6	–3.00	–3.00	–3.00
7	4.00	4.00	4.00
8	6.00	6.00	6.00
9	7.00	7.00	7.00
10	5.00	5.00	5.00
11	9.00	–5.85	1.35
12	–1.00	0.65	–0.15
13	–2.00	1.30	–0.30
14	8.00	–5.20	1.20
15	–3.00	1.95	–0.45
16	4.00	–2.60	0.60
17	6.00	–3.90	0.90
18	7.00	–4.55	1.15
19	5.00	–3.25	0.75

Table 2

Azimuths of the stations and the angles of emergence of first *P*- and *S*-waves (a, b) used for calculation of variations in synthetic *S*-to-*P* intervals

	Az, deg	a, deg	b, deg
RAK	97.00	73.58	40.48
BMR	199.60	78.00	32.06
MEZ	343.30	79.60	28.85

Experiment 1: The impact of the number and configuration of stations

To avoid data inconsistency and bring our simulations closer to reality, we used the same station azimuths and angles of emergence (Table 2) as during the relocation of the Carpathian cluster in Teresva [Gnyp & Malytskyy, 2021]. Velocity v_P was set at 5

and v_S 3 km/s inside the cluster. Since the azimuth of the station is the same for all earthquakes, the tangential changes in the location do not affect the differences in the intervals (Fig. 1), and data from only one station is insufficient. (That is also why the coefficients $a^{(k)}$, $b^{(k)}$, and $c^{(k)}$ in (4) are the same for all pairs of earthquakes.)

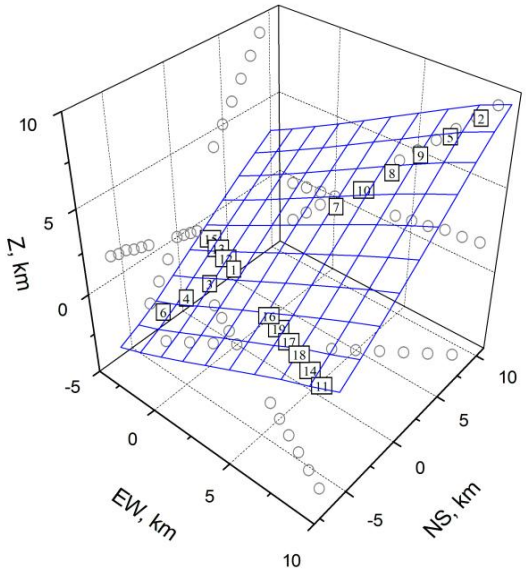

Fig. 2. 3D locations of synthetic earthquakes (Table 1) and the hypothetical rupture plane defined by them. Here and further, the original locations are shown as empty squares, and their projections are shown as empty circles. The locations are approximated by a surface (the blue wire grid) using the method of correlation grids [Davis, 1986].

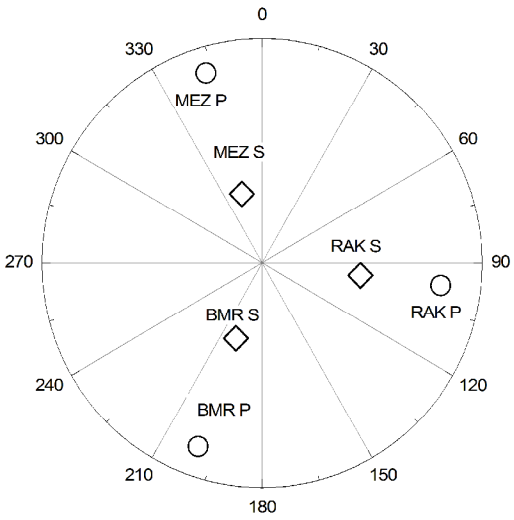

Fig. 3. Azimuths of stations and angles of emergence of first *P*- and *S*-waves (indicated by circles and diamonds, respectively) (Table 2) used for the calculation of variations in the synthetic intervals between *S*- and *P*-waves.

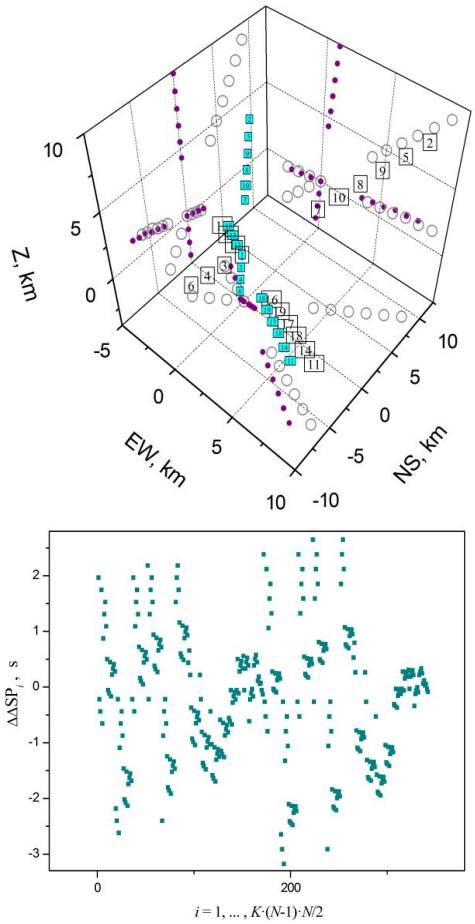

Fig. 4. The locations of earthquakes (Table 1, Fig. 2) recovered based on variations in the synthetic intervals at two stations (RAK and BMR). Here and further, the recovered locations are shown as cyan squares, and their projections are shown as purple circles. At the bottom, the variations in the intervals are plotted.

With two stations, the locations remain not uniquely constrained either. In the case of the BMR and RAK stations, in particular, the rank of the linear system turned out to be deficient, and only the least-squares solution could be estimated (Fig. 4). From the figure, it can be seen that the recovered locations do not exactly coincide with the original ones, although they still lie along the two perfectly straight lines, and in the same sequence, and belong to the same plane defined by the lines (Fig. 5). The entire set of them rotates, however, about the reference earthquake, and its shape is distorted depending, as experiments with other pairs of stations have shown, on the station azimuths and angles of emergence. On the other hand, the variations for the least squares locations turned out to be identical to the original ones with an accuracy of ~ 10^{-15}, which only confirms that the solution is not unique. At the same time, the same least squares locations were obtained each time after the calculations were repeated. This in turn means that at least the least squares solution is unique and stable

and can still appear useful if there are only two stations. In the absence of noise, however, the exact recovery of locations was achieved for all possible configurations of three or more stations (Fig. 6).

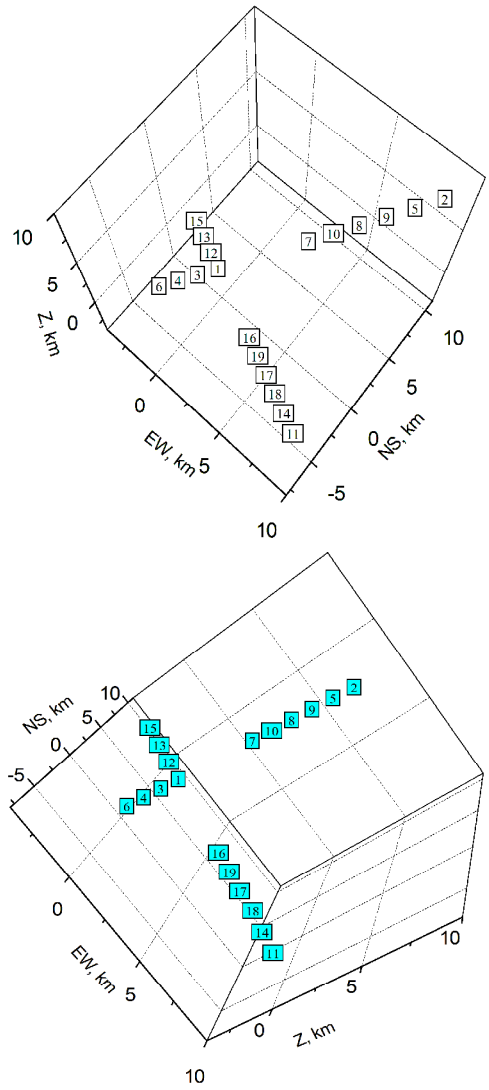

Fig. 5. The sets of original locations (top) and locations recovered based on variations in the intervals at stations RAK and BMR (bottom), the same as in Fig. 4, rotated to better show their similarity.

Experiment 2: The impact of noise

The presence of noise in the observed data was modeled as

$$\mathbf{\Delta\Delta SP^{(n)}} = \mathbf{\Delta\Delta SP^{(o)}} + (0.5 - \mathbf{Ran}) \times r,$$

in which $\mathbf{DDSP^{(n)}}$ are the noised variations in the intervals, $\mathbf{DDSP^{(o)}}$ are the original ones, **Ran** is the vector of random numbers uniformly distributed in the interval between 0 and 1, and r is a coefficient. Since the noise in the travel time differences measured by cross-correlation is independent of their absolute values, we deliberately scaled it by the same factor r.

However, the absolute values of the differences themselves depend on the actual distances between earthquakes, so the same r will result in a relatively higher level of noise for the closer pairs (or for the smaller clusters in general). To be able to compare the results for the clusters of different sizes, we measured the average level of noise using the relative norm:

$$r^* = \left(\sum_{i=1}^{N(N-1)K/2} \left| \Delta\Delta SP_i^{(n)} - \Delta\Delta SP_i^{(o)} \right| / \left| \Delta\Delta SP_i^{(o)} \right| \right) / (N(N-1)K/2).$$

With the same three stations (BMR, MEZU, and RAK) as previously, we then compared the locations recovered for the same synthetic earthquakes at different levels of noise r with their original ones. The locations recovered for r equal to 0.2 and 0.5, as well as the diagrams of $\Delta\Delta SP_i^{(o)}$ and $\Delta\Delta SP_i^{(n)}$, are shown in Figs. 7 and 8. The absolute values of the relative norm r^* were 0.17 and 0.40, respectively. Even at such a high value of r^* as 0.40, the results may only seem satisfactory: although the original lines of synthetic earthquakes are no longer easily recognized, the plane remains almost unperturbed, as does its orientation.

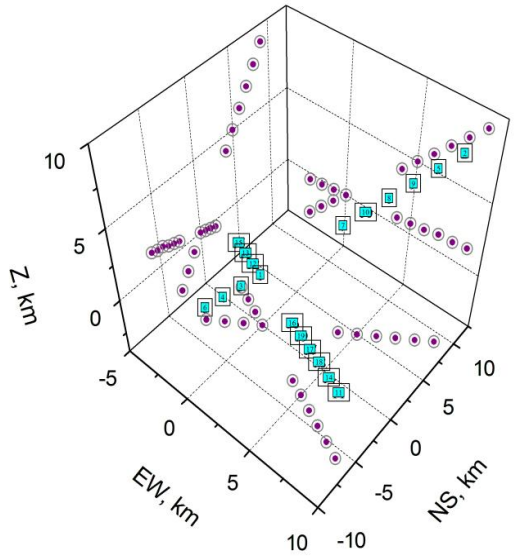

Fig. 6. The locations of earthquakes (Table 1, Fig. 2) recovered based on variations in the synthetic intervals at 3 stations (RAK, BMR, and MEZ).

However, the size of our synthetic cluster (with a side of about 20 km) was rather large, and significantly larger, in particular, than the size of the Teresva cluster of 2015 (with a side about ten times smaller) [Gnyp & Malytskyy, 2021]. So, to get even closer to reality, we downsized our synthetic cluster defined by the same two 3D lines tenfold. The locations were satisfactorily recovered (Fig. 9) with the norm r^* equal to 0.39 (r=0.05) and turned out to be quite similar to the results for the larger cluster with r^* equal to 0.40 (r=0.5).

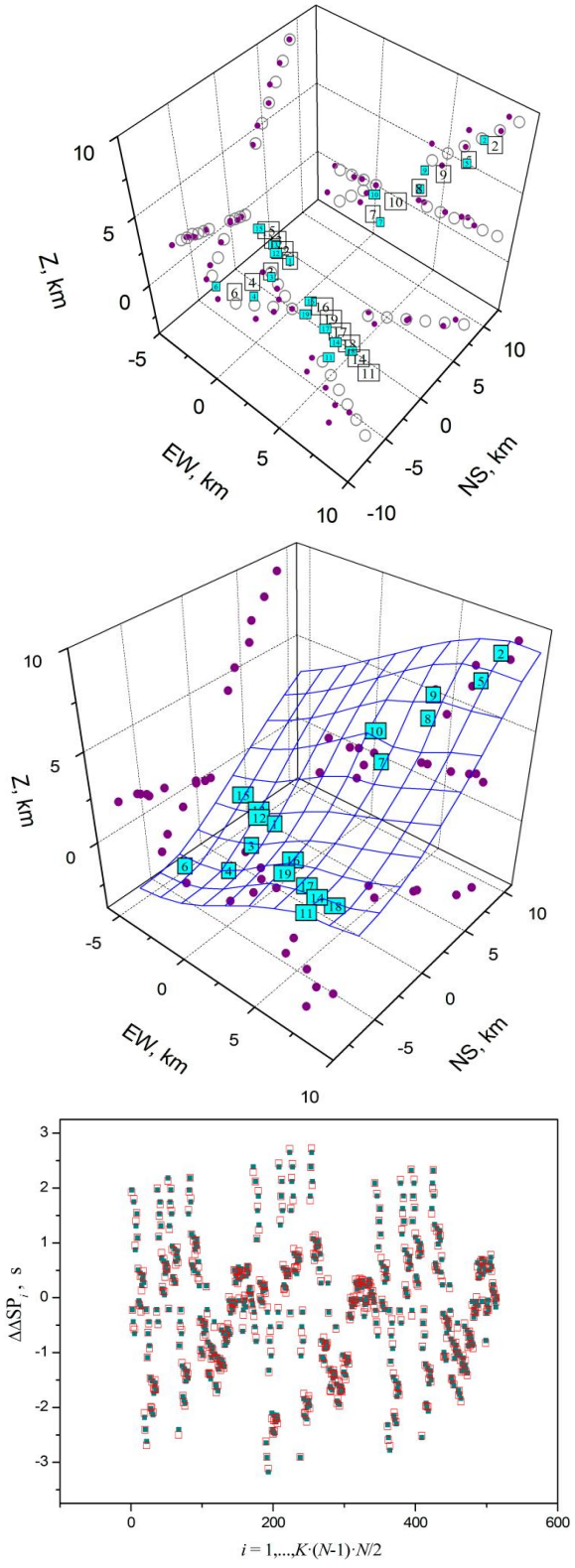

Fig. 7. The locations of earthquakes recovered based on variations in the synthetic intervals at 3 stations (RAK, BMR, and MEZ) in the presence of noise (r=0.2, and r^*=0.17). At the bottom, the original variations are plotted as dark cyan squares, along with the noisy ones plotted here and further on as empty red squares.

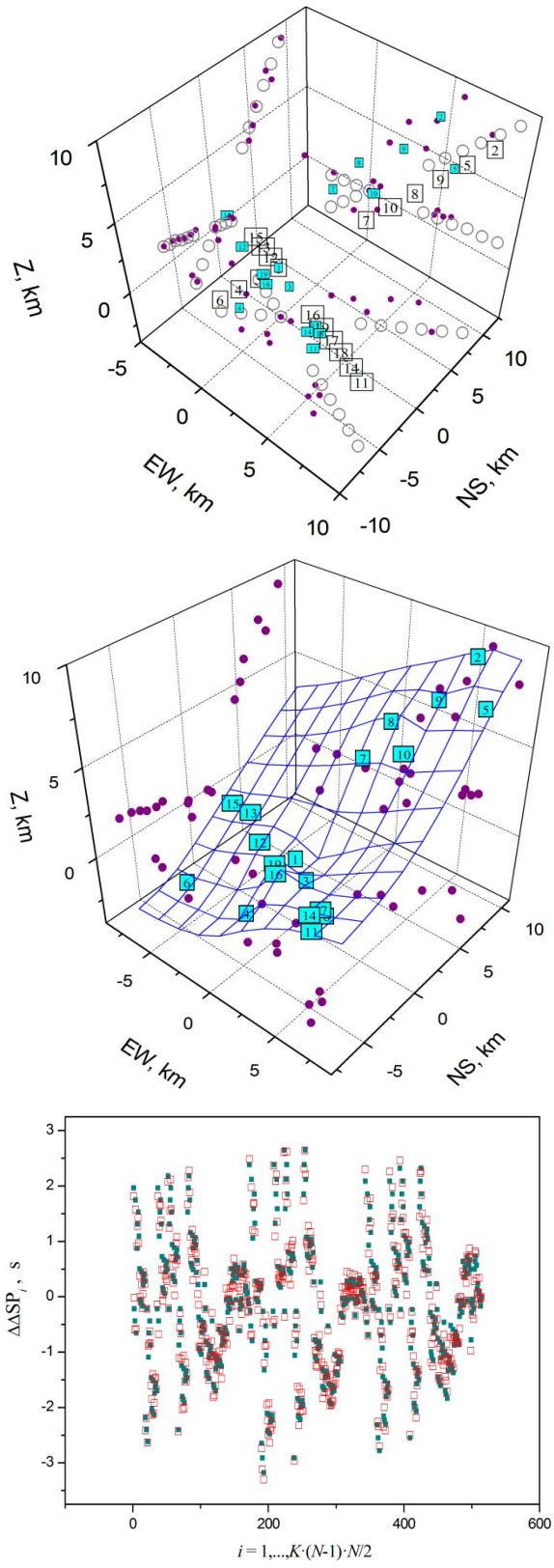

Fig. 8. The locations of earthquakes recovered based on variations in synthetic intervals at 3 stations (RAK, BMR, and MEZ) in the presence of noise (r=0.5, and r^*=0.4). At the bottom, the original variations are plotted, along with the noisy ones.

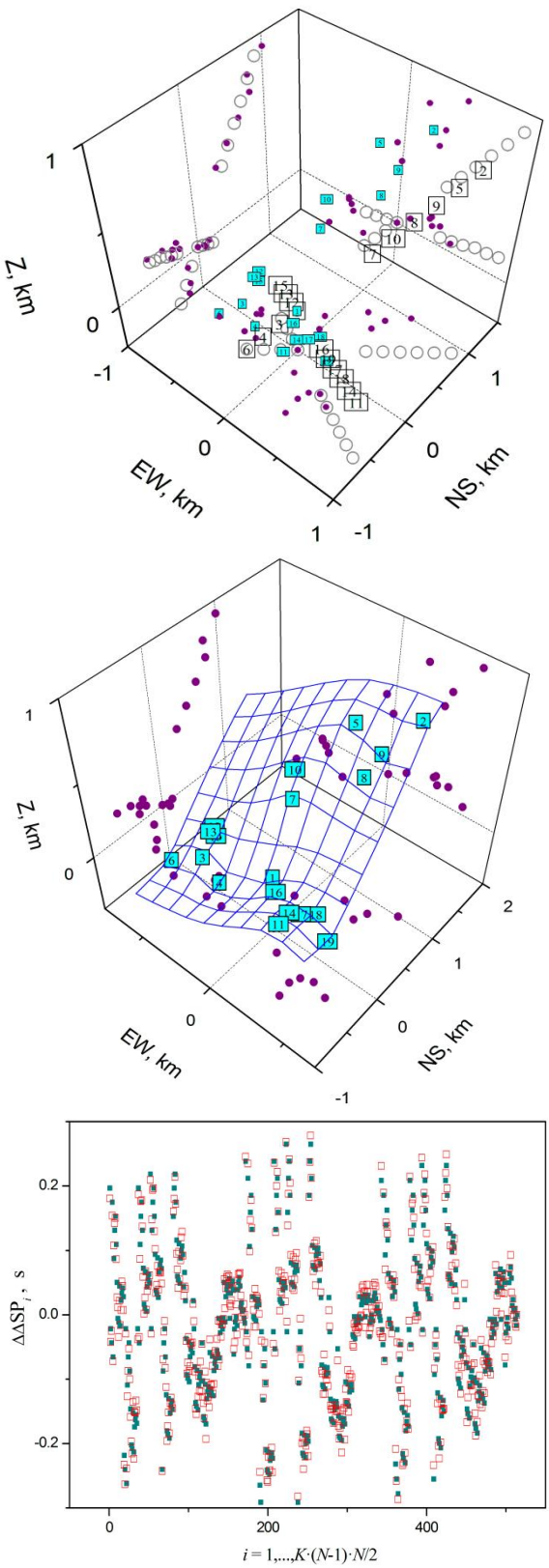

Fig. 9. The 10-fold downscaled coordinates of earthquakes recovered based on variations in synthetic intervals at 3 stations (RAK, BMR, and MEZ) in the presence of noise (r=0.05, and r^*=0.39). At the bottom, the original variations are plotted, along with the noisy ones.

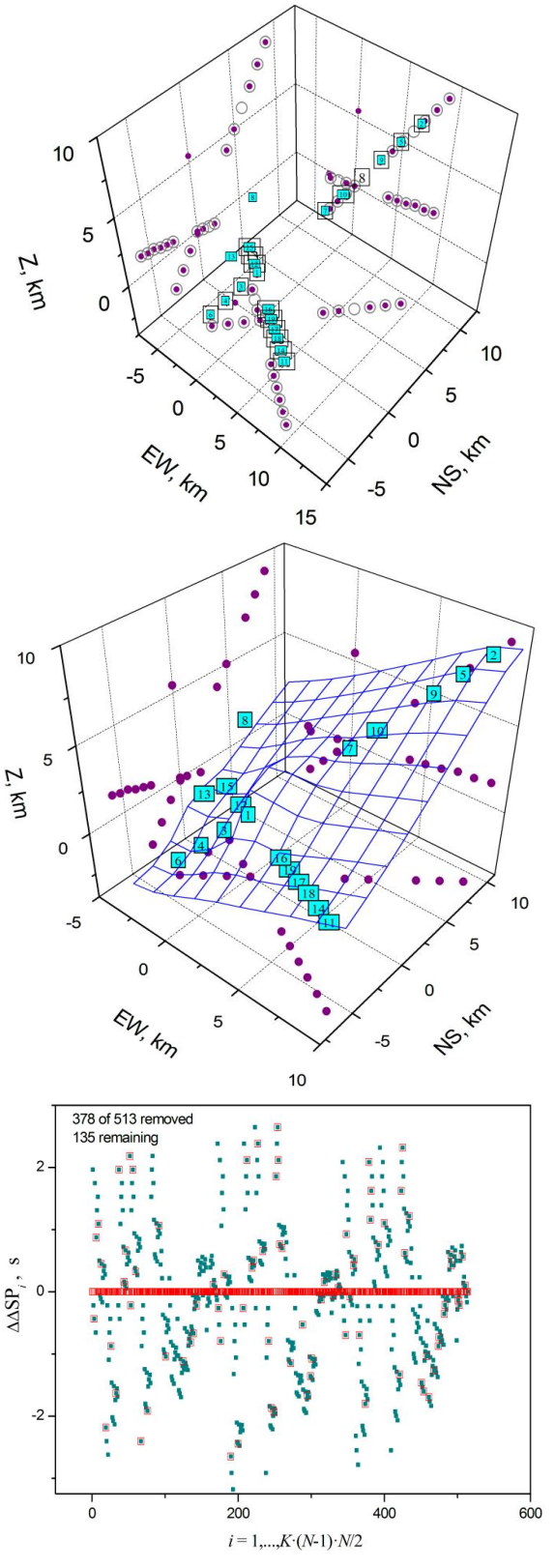

Fig. 10. The locations of earthquakes recovered from a set of variations at 3 stations (RAK, BMR, and MEZ) randomly reduced from 513 to 135. For visualization purposes only, the removed variations are plotted here and further on as zeros.

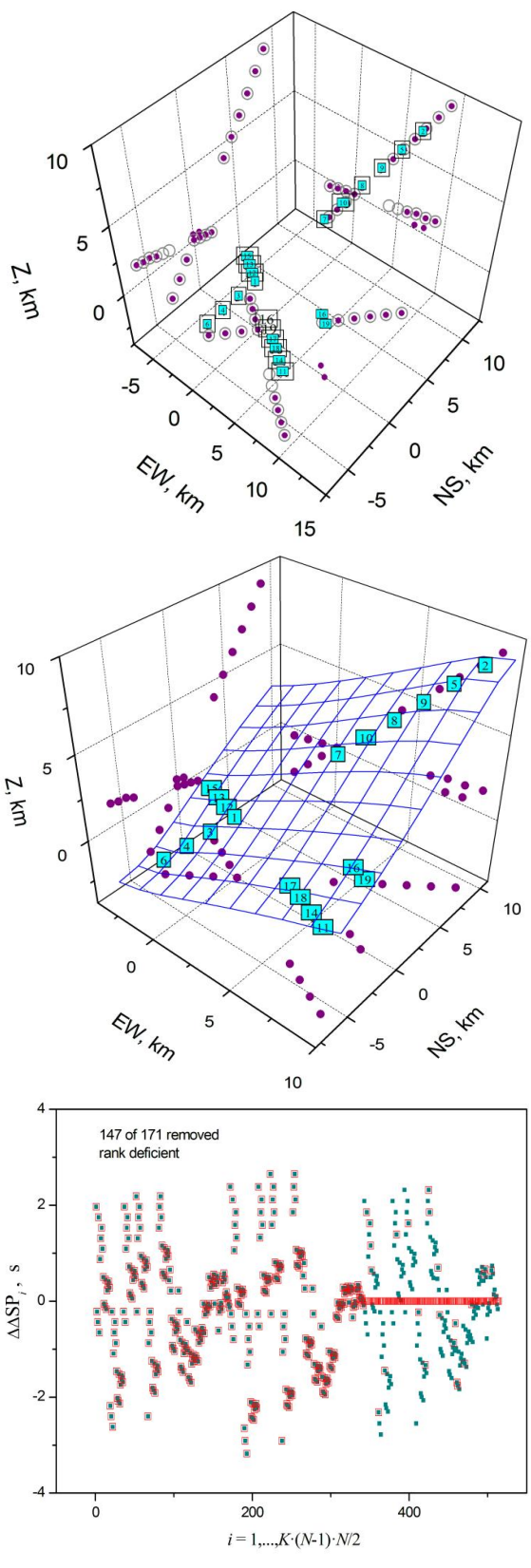

Fig. 11. The locations of earthquakes recovered from a set of variations at 3 stations (RAK, BMR, and MEZ) randomly reduced from 171 to 24 at the station MEZ.

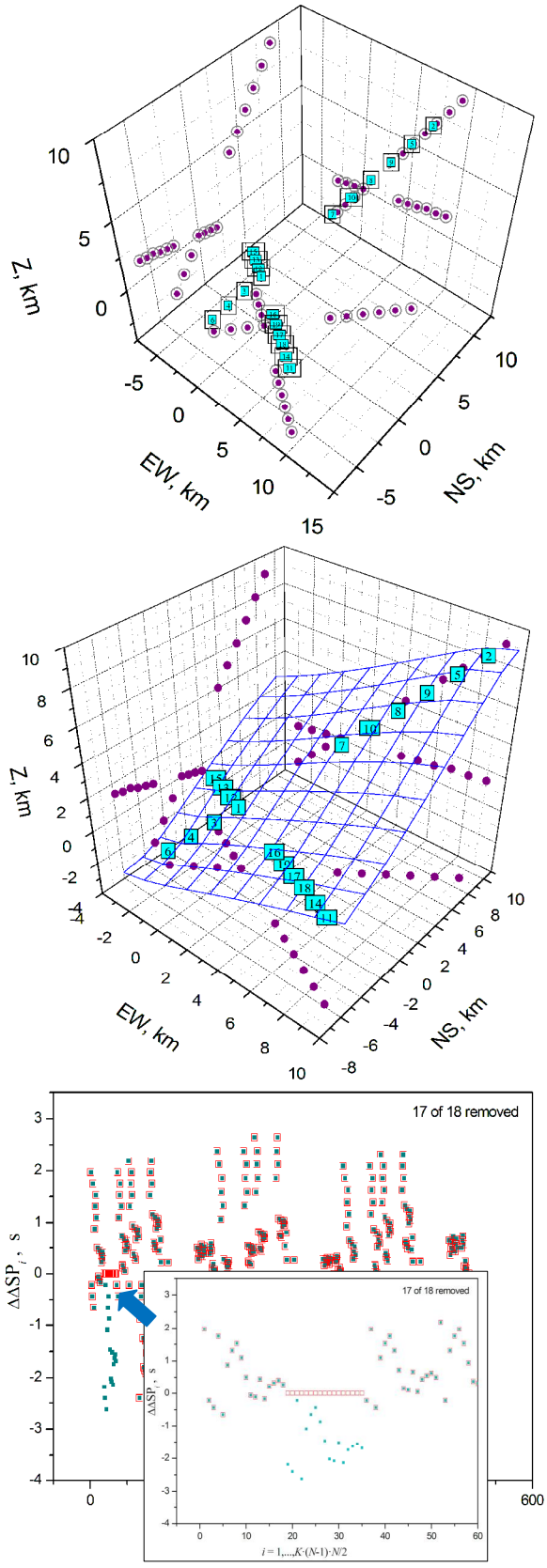

Fig. 12. The locations of earthquakes recovered from a set of variations at 3 stations (RAK, BMR, and MEZ). 17 variations for earthquake 2 are removed from the full set of 18 at the station RAK.

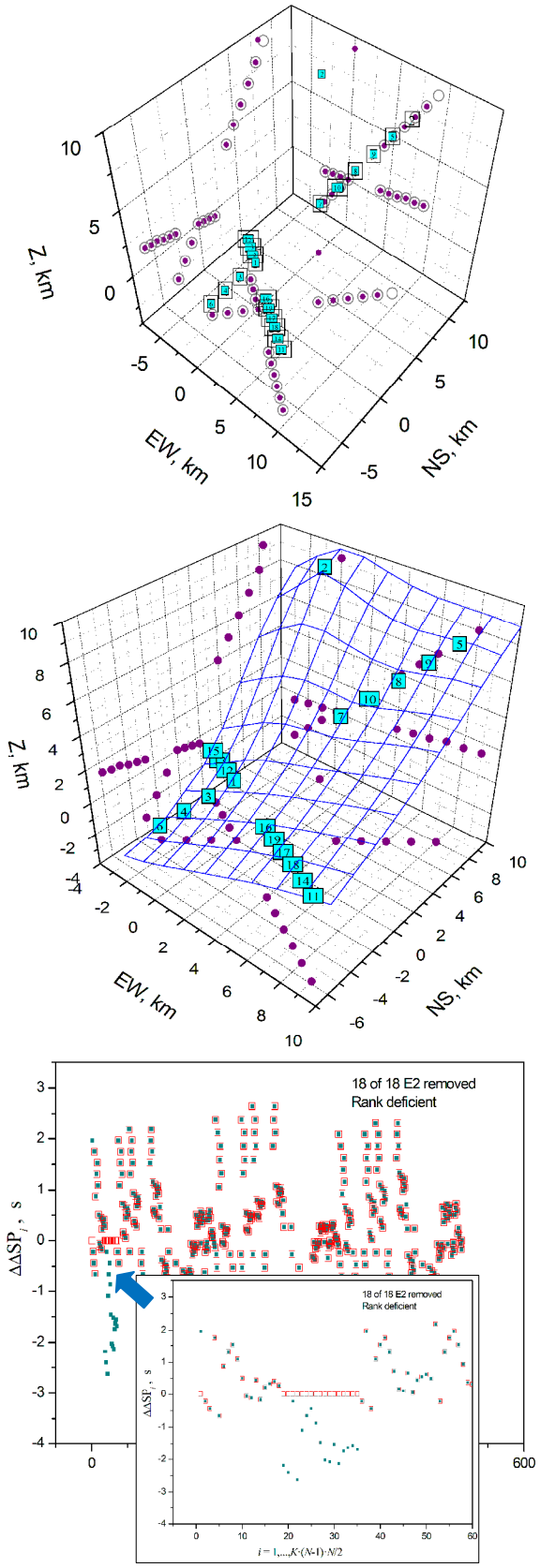

Fig. 13. The locations of earthquakes recovered from a set of variations at 3 stations (RAK, BMR, and MEZ). All variations for earthquake 2 are removed from the full set of 18 at station RAK.

Experiment 3: The impact of sparse data

While *S*- to *P*- intervals varied in the range ±3.5s for the larger cluster in Example 2, for the downsized one they occurred in the range of only ±0.25, the quantity still confidently measurable by cross-correlation (with the HH broadband data, in particular). However, due to the low level of signal-to-noise ratio, it may appear that variations in the intervals cannot be measured with any degree of confidence for some earthquakes. If the number of the corresponding "missing" measurements (*M*) is not very large compared to their largest possible $K\cdot(N-1)\cdot N/2$, such an incomplete system (8) can still remain over-determined and have an exact or approximate solution. So, we tried to establish at what ratio of "missing" intervals, for a single earthquake, a single station, or for all stations (RAK, BMR, and MEZ), the system (2) can become incomplete and, as a result, intractable. For this purpose, *M* random integers uniformly distributed in the interval between 1 and $K\cdot(N-1)\cdot N/2$ (for all earthquakes and all stations), $(N-1)\cdot N/2$ (for a single station), or $N-1$ (for a single earthquake at one station) were generated, and the equations with the corresponding numbers were removed from the full set. Even with a large fraction of "missing" measurements, the locations were recovered almost without a change (Figs. 10–13). Even with 17 variations for earthquake 2 removed from the complete set of 18 at station RAK, its recovered location remained the same (Fig. 12). Only when the number of constraints dropped to zero did the rank of matrix **D** in (8) became deficient, and its location, although still controlled by variations at stations MEZ and BMR, changed (Fig. 13). For earthquake 2, the situation turned out to be similar to experiment 1, where intervals from only two stations were available. Ultimately, it was concluded that the exact recovery of the location is achievable even if at least one direct or indirect link to the reference earthquake is available at three stations; if indirect, however, the link must be through a chain of earthquakes also with three links.

Experiment 4: The impact of inaccurate azimuths and angles of emergence

In this experiment, variations in the synthetic intervals at three stations (again, RAK, BMR, and MEZ) were calculated according to (4) using their original azimuths and the corresponding angles of emergence. Then, to simulate the situation with their inaccurate knowledge, the angles were changed by adding the random numbers to them:

$$Az_i = Az_i^{(o)} + (0.5 - A_i)\times r,$$

$$\alpha_i = \alpha_i^{(o)} + (0.5 - a_i)\times r,$$

$$\beta_i = \beta_i^{(o)} + (0.5 - b_i)\times r,$$

in which angles are measured in radians, $Az_i^{(o)}$, $\alpha_i^{(o)}$, and $\beta_i^{(o)}$ are original azimuths and angles of emergence, A_i, a_i, and b_i are random numbers uniformly distributed in the range between 0 and 1, the coefficient r is the same for all angles, and i = 1, 2, 3. These inaccurate angles were then used for the calculation of locations.

The results for three values of r (0.2, 0.5, and 0.9) are shown in Fig. 14–16. The largest inaccuracies in the respective sets of angles measured in degrees were 5.3˚, 13.1˚, and 23.6˚. Even with such large inaccuracies, the locations were recovered quite satisfactorily, in our opinion, as were the size of the cluster and the orientation of the "rupture" plane defined by them. Again, as in experiment 1, variations in the intervals calculated for the original and inaccurate angles turned out to be virtually identical to within 10^{-15}. This means that the variations can be the same for different sets of angles and locations. And the very idea of recovering angles at the same time as locations looks unrealizable, at least with only three stations.

However, the situation changed with four or more stations: the recovered set of locations became unique, but did not exactly fit the "observed" variations, as would be expected.

Discussion and conclusion

Although the assumptions in the algorithm may seem too numerous or too restrictive, most of them are in fact very realistic and common in seismological practice. Usually, the location and angles of emergence can be calculated by other methods for at least the strongest earthquake used subsequently as a reference. Since the cluster size is assumed to be much smaller than the distance to the stations, which is indeed often the case, it reasonably can be assumed that station azimuths and the angles of emergence are the same for all cluster earthquakes and that the ray paths are the same outside the cluster. Besides, the majority of rays lie in the vertical plane that contains the source and the station, with very few exceptions due to an extremely inhomogeneous velocity structure.

Indeed, various combined experiments with synthetics could be devised to test the performance of the algorithm. However, since their results depended on a large number of factors and in different ways, it had been difficult to separate their impact from each other and arrive at some kind of quantitative measure. So, we varied the configuration of stations, the level of noise in the observed data, their sparsity and inaccuracy of azimuths, and angles of emergence in some tests to extremes until the recovered locations became unrecognizable or were impossible to obtain at all. Even in some extreme tests, recovery of locations was quite satisfactory, in our opinion.

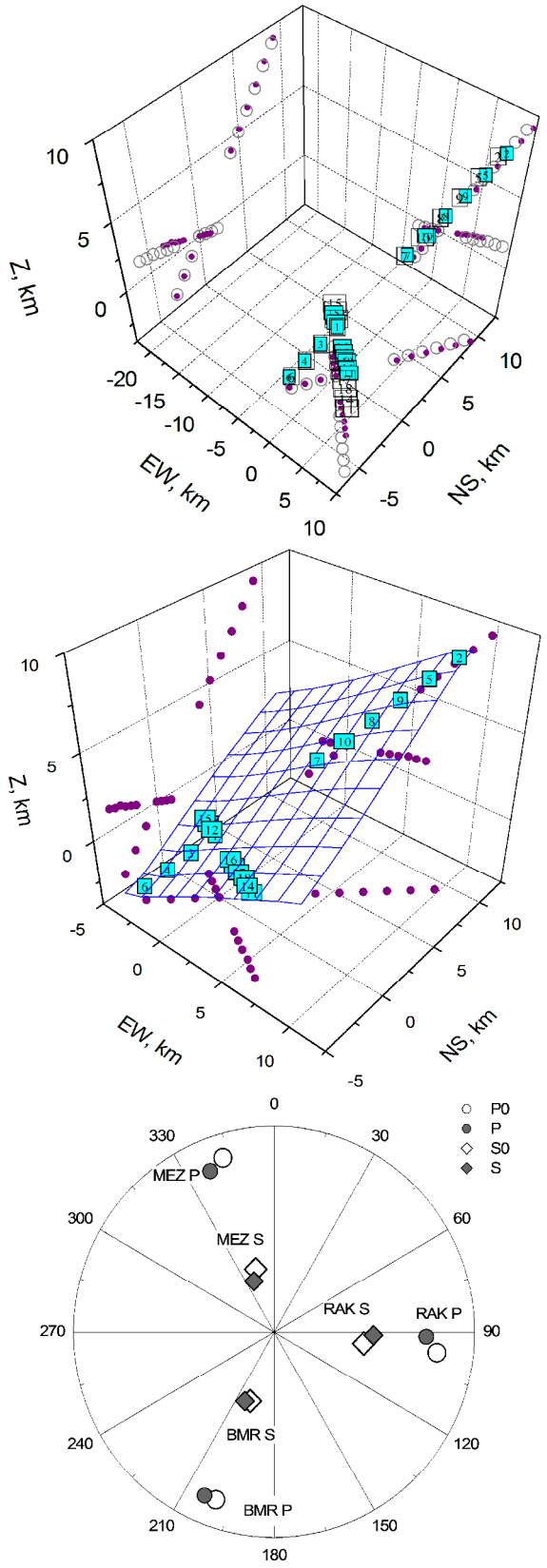

Fig. 14. The locations of earthquakes recovered from a set of variations at 3 stations (RAK, BMR, and MEZ) using inaccurate azimuths and angles of emergence (r=0.2). At the bottom, original (0) and inaccurate angles are plotted.

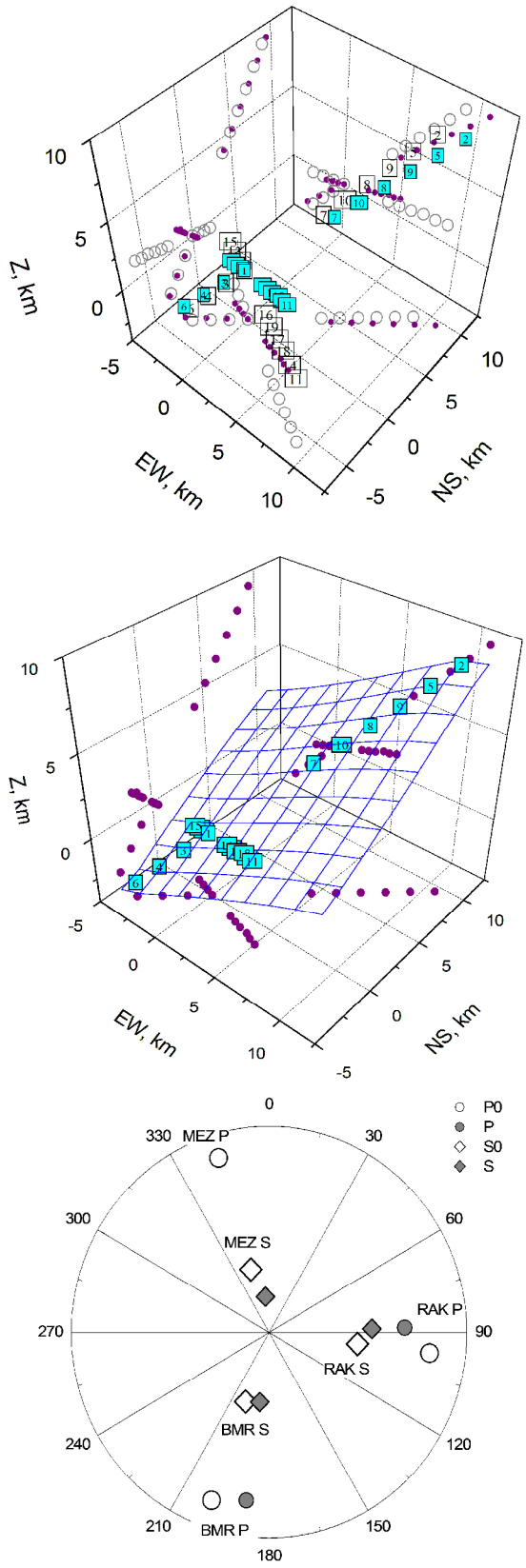

Fig. 15. The locations of earthquakes recovered from a set of variations at 3 stations (RAK, BMR, and MEZ) using inaccurate azimuths and angles of emergence (r=0.5). At the bottom, original (0) and inaccurate angles are plotted.

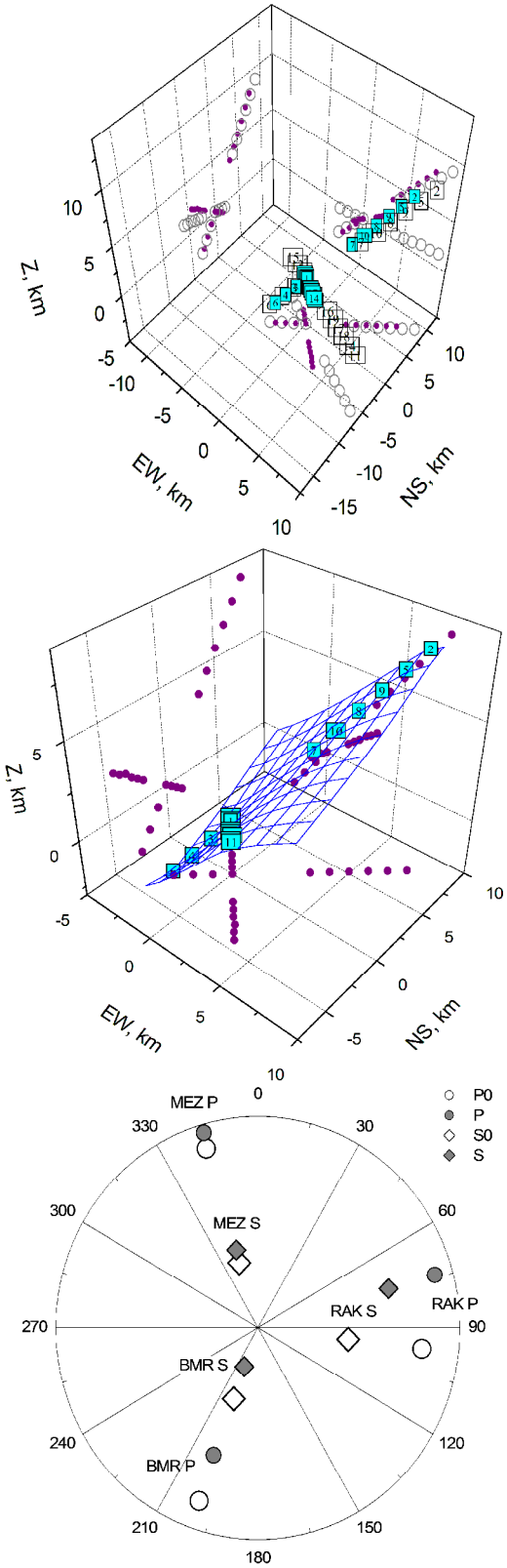

Fig. 16. The locations of earthquakes recovered from a set of variations at 3 stations (RAK, BMR, and MEZ) using inaccurate azimuths and angles of emergence (r=0.9). At the bottom, the original (0) and inaccurate angles are plotted.

An advantage of the algorithm in this regard is that each location is constrained by a much larger number of variations in the intervals than just the arrival times. The exclusion of such a large proportion of uncertainty as the origin times also can be considered an advantage that simplifies the algorithm, making it faster and the results more reliable. The impact of the velocity structure between the source and the station is also reduced to the location of the reference earthquake only. If the absolute location and angles of the emergence of the first *P*- and *S*-waves for the reference earthquake are accurate, the locations of other cluster earthquakes become absolute and accurate as well. However, synthetic experiments have shown that even if the reference was known only approximately, the relative locations of other earthquakes were often recovered to be quite similar to the original ones.

Due to the large number of constraints on each location, the algorithm can be applied primarily in the case of small earthquakes or sparse networks when a large portion of data is missing. The algorithm can be used independently to validate locations determined by other methods, or it can be combined with them to improve their reliability by providing additional constraints. In the next phase, we will apply the algorithm to actual earthquakes and compare the results with those obtained by other techniques.

References

Davis, J. C. (1986). Statistics and Data Analysis in Geology. *John Wiley & Sons, Inc., Second edition*.

Gnyp, A. (2010). Refining locations of the 2005–2006 recurrent earthquakes in Mukacheve, West Ukraine, and implications for their source mechanism and the local tectonics. *Acta Geophysica* 58 (4), 587–603. https://doi.org/10.2478/s11600-010-0006-9

Gnyp, A. (2013). Recovering Relative Locations of the 2005–2006 Mukacheve Earthquakes from Similarity of their Waveforms at a Single Station. *Acta Geophysica* 61 (5), 1074–1087. https://doi.org/10.2478/s11600-012-0096-7

Gnyp, A. (2014). On Reproducibility of Relative Locations of Recurrent Earthquakes Recovered from Similarity of their Waveforms at a Single Station. *Acta Geophysica* 62 (6), 1246–1261. https://doi.org/10.2478/s11600-013-0195-0

Gnyp, A., & Malytskyy, D., (2021). Differential and source terms locations of the 2015 Teresva (East Carpathians) series and their tectonic implications. *Acta Geophysica* 69 (6), 2099–2112. https://doi.org/10.1007/s11600-021-00655-w, https://rdcu.be/cyPNh

Gnyp, A. (2022). Determination of differential locations and focal mechanism of the 2013–2015 earthquakes in Trosnyk, Transcarpatians: methodological aspects and analysis of the results JGD. 2022; Vol. 2(33)2022, No. 2(33), 50–63 DOI: https://doi.org/10.23939/jgd2022.02.050

Harris, D. B., & Douglas, A. D. (2021). The geometry of signal space: a case study of direct mapping between seismic signals and event distribution. *Geophys. J. Int.* 224, 2189–2208. https://doi.org/10.1093/gji/ggaa572

Menke, W. (1999), Using waveform similarity to constrain earthquake locations, *Bull. Seismol. Soc. Am.* 89, 4, 1143–1146. https://doi.org/10.1785/0120130004

Robinson, D. J, Sambridge, M., & Sneider, R. (2007). Constraints on coda wave interferometry estimates of source separation: The acoustic case. *Explor. Geophys*. 38(3), 189–199. https://doi.org/10.1071/EG07019

Robinson, D. J, Sneider, R., & Sambridge, M. Using coda wave interferometry for estimating the variation in source mechanism between double couple events. *J. Geophys. Res*. 112(B12), B12302. https://doi.org/10.1029/2007JB004925

Robinson, D. J, Sambridge, M., Sneider, R., & Hauser, J. (2013). Relocating a Cluster of Earthquakes Using a Single Seismic Station. *Bull. Seism. Soc. Am.* 108(6), 3057–3072. https://doi.org/10.1785/0120130004

Shearer, P. M. (1997). Improving local earthquake locations using L1 norm and waveform cross-correlation: Application to the Whittier Narrows, California, aftershock sequence. *J. Geophys. Res.* 102(B4), 8269–8283. https://doi.org/10.1029/96JB03228

Shearer, P., Hauksson, E., & Lin, G. (2005). Southern California hypocenter relocation with waveform cross-correlation. Part 2: Results using source-specific station terms and cluster analysis. *Bull. Seism. Soc. Am.* 95(3), 904–915. https://doi.org/10.1785/0120040168

Snieder, R., and M. Vrijlandt (2005), Constraining the source separation with coda wave interferometry: Theory and application to earthquake doublets in the Hayward Fault, California, J. Geophys. Res., 110,B04301, doi:10.1029/2004JB003317.

Waldhauser, F, & Ellsworth, L. W. (2000). A Double-Difference Earthquake Location Algorithm: Method and Application to the Northern Hayward Fault. California. *Bull. Seism. Soc. Am.* 90(6), 1353–1368. https://doi.org/10.1785/0120000006

Appendix 1

The structure of the matrices in equation (7)

$da^{(k)}$	$db^{(k)}$	$dc^{(k)}$	0	0	0	0	0	0	⋯	0	0	0	0	0	0	0	0	0		x_2		$DDSP^{(k)}_{12}$
0	0	0	$da^{(k)}$	$db^{(k)}$	$dc^{(k)}$	0	0	0	⋯	0	0	0	0	0	0	0	0	0		y_2		$DDSP^{(k)}_{13}$
0	0	0	0	0	0	$da^{(k)}$	$db^{(k)}$	$dc^{(k)}$	⋯	0	0	0	0	0	0	0	0	0		z_2		$DDSP^{(k)}_{14}$
⋮	⋮	⋮	⋮	⋮	⋮	⋮	⋮	⋮	⋱	⋮	⋮	⋮	⋮	⋮	⋮	⋮	⋮	⋮		x_3		⋮
0	0	0	0	0	0	0	0	0	⋯	0	0	0	0	0	0	$da^{(k)}$	$db^{(k)}$	$dc^{(k)}$		y_3		$DDSP^{(k)}_{1N}$
$-da^{(k)}$	$-db^{(k)}$	$-dc^{(k)}$	$da^{(k)}$	$db^{(k)}$	$dc^{(k)}$	0	0	0	⋯	0	0	0	0	0	0	0	0	0		z_3		$DDSP^{(k)}_{23}$
$-da^{(k)}$	$-db^{(k)}$	$-dc^{(k)}$	0	0	0	$da^{(k)}$	$db^{(k)}$	$dc^{(k)}$	⋯	0	0	0	0	0	0	0	0	0		x_4		$DDSP^{(k)}_{24}$
$-da^{(k)}$	$-db^{(k)}$	$-dc^{(k)}$	0	0	0	0	0	0	⋯	0	0	0	0	0	0	0	0	0		y_4		$DDSP^{(k)}_{25}$
⋮	⋮	⋮	⋮	⋮	⋮	⋮	⋮	⋮	⋱	⋮	⋮	⋮	⋮	⋮	⋮	⋮	⋮	⋮		z_4		⋮
$-da^{(k)}$	$-db^{(k)}$	$-dc^{(k)}$	0	0	0	0	0	0	⋯	0	0	0	0	0	0	$da^{(k)}$	$db^{(k)}$	$dc^{(k)}$		⋮		$DDSP^{(k)}_{2N}$
0	0	0	$-da^{(k)}$	$-db^{(k)}$	$-dc^{(k)}$	$da^{(k)}$	$db^{(k)}$	$dc^{(k)}$	⋯	0	0	0	0	0	0	0	0	0	´	x_{N-2}	=	$DDSP^{(k)}_{34}$
0	0	0	$-da^{(k)}$	$-db^{(k)}$	$-dc^{(k)}$	0	0	0	⋯	0	0	0	0	0	0	0	0	0		y_{N-2}		$DDSP^{(k)}_{35}$
0	0	0	$-da^{(k)}$	$-db^{(k)}$	$-dc^{(k)}$	0	0	0	⋯	0	0	0	0	0	0	0	0	0		z_{N-2}		$DDSP^{(k)}_{36}$
⋮	⋮	⋮	⋮	⋮	⋮	⋮	⋮	⋮	⋱	⋮	⋮	⋮	⋮	⋮	⋮	⋮	⋮	⋮		x_{N-1}		⋮
0	0	0	$-da^{(k)}$	$-db^{(k)}$	$-dc^{(k)}$	0	0	0	⋯	0	0	0	0	0	0	$da^{(k)}$	$db^{(k)}$	$dc^{(k)}$		y_{N-1}		$DDSP^{(k)}_{3N}$
0	0	0	0	0	0	$-da^{(k)}$	$-db^{(k)}$	$-dc^{(k)}$	⋯	0	0	0	0	0	0	0	0	0		z_{N-1}		$DDSP^{(k)}_{45}$
0	0	0	0	0	0	$-da^{(k)}$	$-db^{(k)}$	$-dc^{(k)}$	⋯	0	0	0	0	0	0	0	0	0		x_N		$DDSP^{(k)}_{46}$
0	0	0	0	0	0	$-da^{(k)}$	$-db^{(k)}$	$-dc^{(k)}$	⋯	0	0	0	0	0	0	0	0	0		y_N		$DDSP^{(k)}_{47}$
⋮	⋮	⋮	⋮	⋮	⋮	⋮	⋮	⋮	⋱	⋮	⋮	⋮	⋮	⋮	⋮	⋮	⋮	⋮		z_N		⋮
0	0	0	0	0	0	$-da^{(k)}$	$-db^{(k)}$	$-dc^{(k)}$		0	0	0	0	0	0	$da^{(k)}$	$db^{(k)}$	$dc^{(k)}$				$DDSP^{(k)}_{4N}$
⋮	⋮	⋮	⋮	⋮	⋮	⋮	⋮	⋮	⋱	⋮	⋮	⋮	⋮	⋮	⋮	⋮	⋮	⋮				⋮
0	0	0	0	0	0	0	0	0	⋯	$-da^{(k)}$	$-db^{(k)}$	$-dc^{(k)}$	da^k	db^k	dc^k	0	0	0				$DDSP^{(k)}_{N-2\ N-1}$
0	0	0	0	0	0	0	0	0	⋯	$-da^{(k)}$	$-db^{(k)}$	$-dc^{(k)}$	0	0	0	$da^{(k)}$	$db^{(k)}$	$dc^{(k)}$				$DDSP^{(k)}_{N-2\ N}$
0	0	0	0	0	0	0	0	0	⋯	0	0	0	$-da^{(k)}$	$-db^{(k)}$	$-dc^{(k)}$	$da^{(k)}$	$db^{(k)}$	$dc^{(k)}$				$DDSP^{(k)}_{N-1\ N}$

Андрій ГНИП, Дмитро МАЛИЦЬКИЙ

Карпатське відділення Інституту геофізики ім. С.І. Субботіна НАН України, вул. Наукова, 3Б, Львів, 79060, Україна, ел. пошта: agnyp.gm@gmail.com, https://orcid.org/0000-0002-2612-4234

ВИЗНАЧЕННЯ КООРДИНАТ ЗЕМЛЕТРУСІВ У КЛАСТЕРАХ НА ОСНОВІ ВАРІАЦІЙ ІНТЕРВАЛІВ МІЖ ВСТУПАМИ *P*- ТА *S*-ХВИЛЬ

Довжину інтервалу між першими вступами *P*- та *S*-хвиль часто використовують для приблизного оцінювання епіцентральної відстані. Ми пропонуємо алгоритм визначення координат землетрусів із одночасним порівнюванням великої кількості таких інтервалів. Для визначення різниці між інтервалами на кожній зі станцій обчислюється функція взаємної кореляції між відповідними хвильовими формами – без визначення абсолютної довжини інтервалів. У поточній версії алгоритму припускаємо, що розміри кластера набагато менші за відстань до станцій; азимути станцій і кути виходу перших *P*- та *S*-хвиль доволі точно відомі, принаймні для одного (опорного) землетрусу; промені перших хвиль лежать у вертикальній площині, що містить вогнище і станцію. Зв'язок між координатами і різницею довжини інтервалів у цьому разі стає суто геометричним і лінійним, а відповідну систему рівнянь легко розв'язати. Результати серії модельних експериментів з використанням різної кількості станцій та їхньої конфігурації, рівня шуму у спостережених даних, ступеня неповноти даних, неточних азимутів та кутів виходу довели стійкість і надійність алгоритму і можливість його застосування надалі до реальних даних. З огляду на велику кількість обмежень на координати кожного із землетрусів алгоритм найдоцільніше використовувати у разі дуже слабких землетрусів або малої кількості станцій, коли істотна частина даних відсутня. Алгоритм можна використовувати окремо – або з метою підтвердження правильності координат, визначених іншими методами, або вбудувати його в інші методи, щоб підвищити їх надійність завдяки істотному збільшенню кількості обмежень.

Ключові слова: координати землетрусів; визначення координат; кластер землетрусів; інтервал між вступами *P*- та *S*-хвиль; функція взаємної кореляції.

Received 19.09.2023